Pramana – J. Phys. (2017) 89:2
DOI 10.1007/s12043-017-1395-y
© Indian Academy of Sciences

The effects of different possible modes of uniaxial strain on the tunability of electronic and band structures in MoS_2 monolayer nanosheet via first-principles density functional theory

DIMPLE[1], NITYASAGAR JENA[1], SHOUNAK DHANANJAY BEHERE[2] and ABIR DE SARKAR[1,*]

[1]Institute of Nano Science and Technology, Phase 10, Sector 64, Mohali 160 062, India
[2]National Institute of Technology, Ravangla Campus, Barfung Block, Ravangla Sub-Division, Sikkim 737 139, India
*Corresponding author. E-mail: abirdesarkar@gmail.com; abir@inst.ac.in

Published online 19 June 2017

Abstract. *Ab-initio* density functional theory-based calculations have been performed on monolayer (ML) MoS_2 nanosheet to study the variation of its electronic properties with the application of uniaxial tensile and compressive strain along its two non-equivalent lattice directions, namely, the zig-zag and the arm-chair directions. Among all the strain types considered in this study, uniaxial tensile strain applied along the zig-zag direction is found to be the most efficacious, inducing a greater tunability in the band gap over a large energy range (from 1.689 to 0.772 eV corresponding to 0–9% of applied strain), followed by uniaxial tensile strain along arm-chair direction. In contrast, the ML–MoS_2 nanosheet is found to be less sensitive to the compressive strain applied uniaxially along both the arm-chair as well as zig-zag directions. Moreover, the charges on Mo and S atoms are not found to undergo considerable changes under the application of uniaxial strain, as the atomic motion along the other direction is free from any constraint.

Keywords. *Ab-initio* density functional theory; band gap; monolayer MoS_2 nanosheet; strain.

PACS Nos **31.15.E–; 31.15.eg; 71.15.Mb; 71.20.–b; 73.20.At; 61.46.+w; 73.22.–f**

1. Introduction

Synthesizing novel materials at the nanoscale whose electrical properties can be controlled to a high level of precision is vital for a wide range of applications. Experimental realization of atomically thin two-dimensional nanomaterials like graphene by mechanical exfoliation, has revealed amazing electromechanical properties in these materials in their low-dimensional structures which is not observed in their bulk form. This has motivated the scientific community to explore layered nanostructures which meet two essential criteria: physically isolable and thermodynamically stable in ambient conditions [1–3]. In league with graphene, the next potential candidates are the two-dimensional transition-metal-dichalcogenides (TMDCs) which have currently drawn a surge in research interests. The TMDCs have the chemical formula MX_2, where M is a transition metal element (Mo, W etc.) and X is a chalcogen (S, Se, Te). A single layer of it has a thickness of 6–7 Å with strong in-plane covalent bonding [4]. Owing to the excellent mechanical properties, the two-dimensional TMDCs have the capability of withstanding a significant amount of strain and sustaining the elastic deformations before fracture, thereby presenting an encouraging concept of strain engineering [5]. Local strain modulates the band-gap, electrical and other related properties of the TMDCs, the reason being the entanglement or correlation in their diverse properties, such as electronic, optical, mechanical, chemical and thermal properties [6]. Moreover, MoS_2 is put to a distinctive advantage by virtue of its semiconducting properties which allow it to overcome the shortcomings of graphene, viz. zero band gap, lack of clear current and low switching capacity, thereby opening the possibilities for vivid electronic, optoelectronic and photovoltaic applications [7]. A unique property which characterizes TMDCs is the transition from indirect to direct band gap when it is scaled down from bulk to monolayer form. It is experimentally reported that for MoS_2 layers, the indirect band gap of 1.2 eV in bulk widens to a direct band gap of 1.9 eV in monolayer nanosheet [8]. To push the Moore's law even further, the direct and tunable band gaps of MoS_2 which are even wider than silicon

is of prime advantage which suppresses the source-to-drain tunnelling at the scaling limit of transistors [9]. Strongly correlated electron phenomena, such as charge density waves and superconductivity are also exhibited by ML–MoS_2 [10]. Building ML–MoS_2-based logic circuits and memory devices operable at room temperatures with low standby power can be easily envisioned [11,12]. The development of TMDCs has got immense scope for applications in spintronic devices, photocatalysis and quantum computing [13]. The strain application in TMDCs like MoS_2 potentially paves the way for the application of these nanomaterials in high-performance transistors and strain sensors [14].

Unlike graphene, TMDCs exist in many different structural phases depending on the position of chalcogenide atom with respect to the transition metal atom, e.g., 2H, 1T, etc. The monolayer polytypes of TMDCs can show up in several forms with varying degrees of stability: trigonal prismatic with honeycomb motif (D_{3h} point group) is referred to as 2H- and 1H-phase, while octahedral (D_{3d} point group) is designated as the 1T-phase. In our study, we have considered the 1H phase of MoS_2 which is its most stable one [4,15,16]. The properties of ML TMDCs like MoS_2 can be altered or modified by various means, viz., varying the number of layers of MoS_2, chemical treatments, doping, nanopatterning, application of external electric field, engineering defects, application of mechanical strain, etc. The properties of MoS_2 do not show a smooth variation with the number of layers. Moreover, the other ways adopted to manipulate the electronic properties are accompanied by enormous hassles including harsh treatments, which induce permanent changes in its structure as well as properties. Among all the aforementioned avenues, strain engineering turns out to be the most benign and optimum one in tuning the band gap as it allows to work on the pristine nanostructure without bringing about any permanent change in the nanostructure or its properties [5]. Furthermore, within the elastic limit, the withdrawal of mechanical strain restores the nanosheet to its initial structure [17]. Kaewmaraya *et al* demonstrated strain-induced tunability in the optical and photocatalytic properties in monolayer ZnO nanosheets [18]. Moreover, Liu *et al* have noted a shear strain-induced transition in indirect band gap to a direct one in AlN monolayer nanosheet [19]. Furthermore, application of mechanical strain has also been found to be very effective in enhancing the storage capacity in energy materials [20,21]. Biaxial homogeneous strain is routinely studied in band-gap engineering in nanostructures and the role of uniaxial strain is relatively less studied.

The purpose of this paper is to highlight the efficacy of uniaxial strain in tuning band gap in ML–MoS_2 nanosheet. To this end, uniaxial mechanical strain has been applied on ML–MoS_2 nanosheet for a systematic investigation on the variation in its electronic properties and charge density with uniaxial strain. In this work, band gap in single-layer MoS_2 nanosheet has been engineered by subjecting atomically thin ML–MoS_2 nanosheet to uni-axial tensile strain and compressive strain along two non-equivalent crystal directions, namely, the zig-zag and the arm-chair directions. An ultrafine tuning in the band gap and the concomitant transition in the band gap from direct to indirect under the application of strain as observed in our work is of utmost importance in guiding the development of strain sensors and futuristic nanoelectronic devices.

2. Computational methodology

An infinite 2D ML–MoS_2 nanosheet has been modelled in a supercell with rectangular symmetry, as shown in figure 1. The supercell consists of six atoms (two for Mo and four for S). One of the lattice vectors is aligned along the zig-zag (ZZ) direction, while the other lies along the arm-chair (AC) direction. First-principles density functional theory (DFT) [22,23] based calculations, as implemented in the Vienna *ab-initio* simulation package (VASP) [24–26], have been performed. Projector-augmented wave (PAW) [27] pseudopotentials within the generalized gradient approximations (GGA) [28] for the exchange correlation functional of Perdew–Burke–Ernzerhof (PBE) [29] have been used in our theoretical investigations. Six electrons of Mo ($4d^5 5s^1$) and six electrons of S ($3s^2 3p^4$) have been treated as valence electrons. The energy cut-off for the plane wave basis set was set at 520 eV and a Γ-centred $16 \times 9 \times 1$ K-mesh has been used for the Brillouin zone integration. A vacuum thickness of about 15 Å has been used to decouple the periodic images of the nanosheets repeated along z-direction. Structural optimizations based on the conjugate gradient scheme have been performed and atomic positions have been allowed to relax until the Hellman–Feymann forces on atoms reached less than 0.02 eV/Å.

The supercell shown in figure 1 was optimized as a whole, i.e., the lattice constants as well as the atomic positions. The optimized nanosheet of ML–MoS_2 exhibits a trilayer structure in which the Mo layer is sandwiched between two S layers. The equilibrium lattice constant and Mo–S bond length obtained from the generalized gradient approximation (GGA-PBE) are found to be 3.18 and 2.41 Å respectively, which are in good agreement with the experimental data [30]. Upon geometry optimization, the band structure of ML–MoS_2 nanosheet was calculated by using the charge

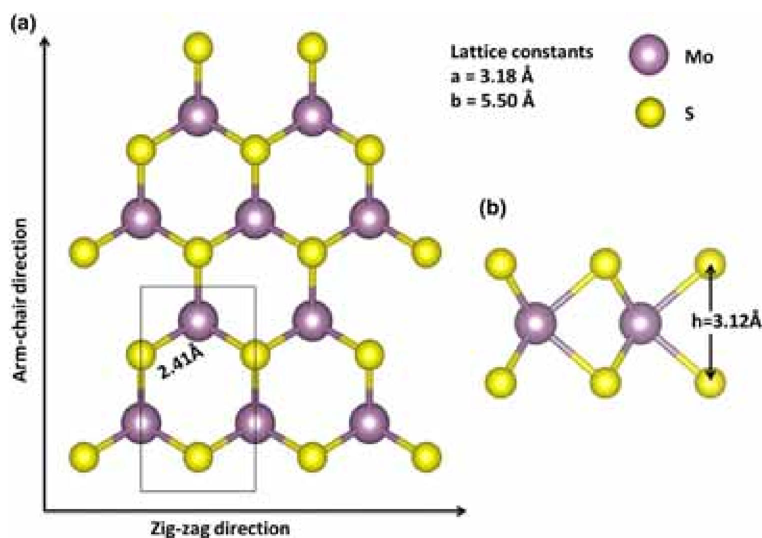

Figure 1. Ball and stick model for atomic structure of MoS_2−ML nanosheet in a rectangular supercell. **(a)** Top view and **(b)** side view.

density obtained from geometry optimization calculations. Band structure computed in this manner shows a direct band gap of 1.69 eV at the K-point which also agrees well with other theoretical and experimental studies [31,32]. In a similar vein, we have also performed calculations for all other types of uniaxially strained ML–MoS_2 nanosheets. Lattice constant has been scaled up and down in steps of 1% up to 9%, in order to account for tensile and compressive strain, respectively. In the calculations on the strained sheets, the atomic positions have only been relaxed, while the lattice constants have been held.

3. Results and discussion

In our computations, the strain-free ML–MoS_2 nanosheet is found to be a direct band-gap semiconductor showing a band gap of 1.689 eV with conduction band minimum (CBM) and the valence band maximum (VBM) occurring at the high-symmetry K point of the Brillouin zone (BZ), which is in excellent agreement with all other theoretical studies [31]. The variation in the band structure with the application of strain along the high symmetry points of the BZ as Γ, K, M, Γ, is shown in figure 2. First-principles based phonon dispersion calculations have confirmed the stability of ML–MoS_2 nanosheet up to 9% of applied strain [31] and hence, the range of strain studied in this work.

From figure 3, it is obvious that the band gap decreases almost linearly from 1.689 to 0.772 eV with tensile strain applied uniaxially along the zig-zag direction corresponding to 0–9% of the tensile strain and the band gap is found to change from direct to indirect. However, the modulation in band gap is less significant under compressive strain applied along zig-zag and arm-chair directions as viewed in figure 3. For uniaxial compressive strain applied along zig-zag direction, band gap increases from 1.689 to 1.822 eV with the application of strain from 0 to 3%. Then, the band gap gradually decreases from 1.822 to 1.367 eV for a further increase in strain from 3 to 9%. Similar observation has been made in the case of uniaxial compressive strain applied along arm-chair direction. Band gap is found to increase when strain goes from 0 to 4%. Thereafter, the band gap progressively drops to 1.63 eV when strain increases from 4 to 9%. However, in both the cases, the band gap remains direct up to 0–7% of applied strain; while for strain exceeding 7%, the band gap turns indirect as depicted in figure 3. Similar to the uniaxial tensile strain along the zig-zag direction, a notable decrement in the band gap has been noticed for uniaxial tensile strain applied along arm-chair direction, which summarizes that uniaxial tensile strain applied along both the zig-zag and arm-chair directions bring about greater tunability in the band gap as well as band structure of ML–MoS_2 nanosheet (table 1).

The electronic charge density plot for ML–MoS_2 and uniaxial strained system is shown in figure 4. Corresponding to the application of uniaxial tensile strain, the spatial extent of the isosurfaces are found to extend into the bonding region showing some overlap between the isosurfaces centred on adjacent atoms, as compared to the strain free ML–MoS_2 nanosheet. A slight contraction in the isosurface in the atomic regions is observed in the case of compressive strain, with respect to the unstrained ML–MoS_2 nanosheets. The Bader charge analysis has also been performed on unstrained

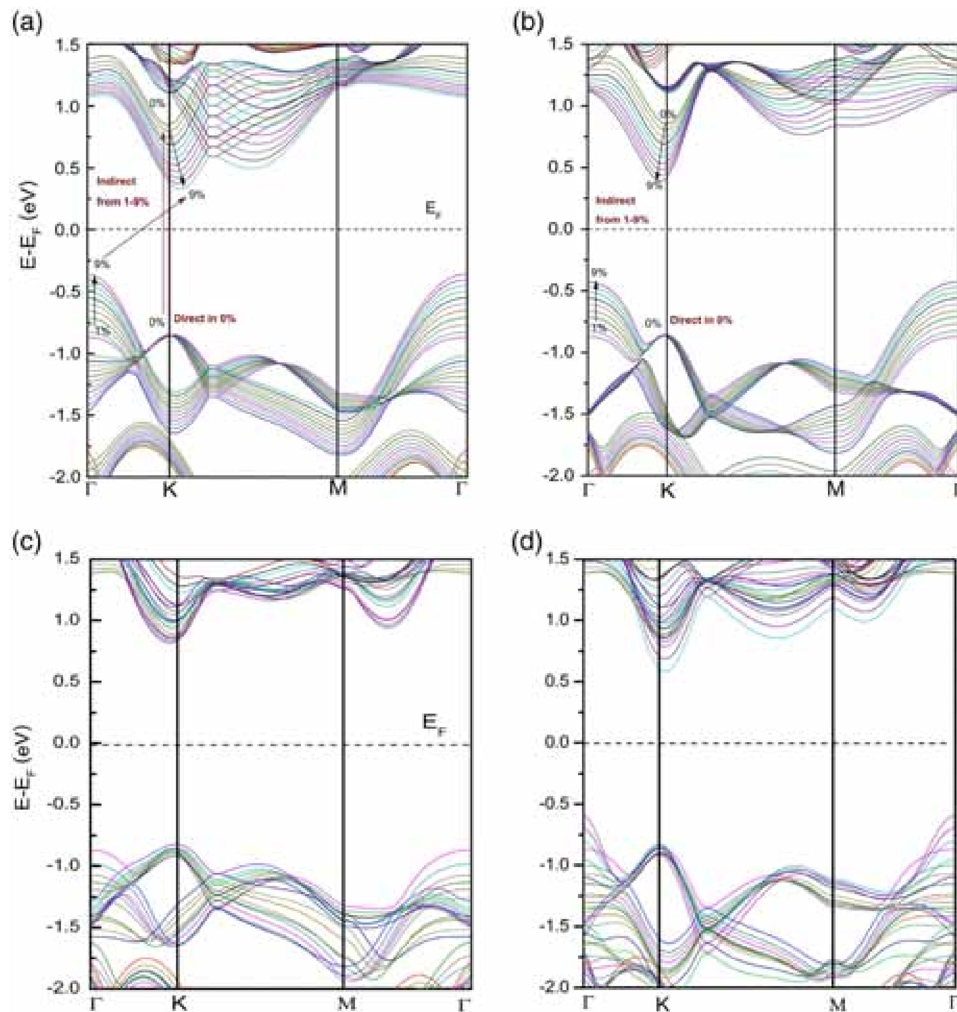

Figure 2. Variation of electronic band structure of ML–MoS_2 under different uniaxial strain (0–9%) applied uniaxially along the zig-zag and arm-chair directions respectively. The band gap decreases with the increase in strain and it turns indirect under tensile strain and direct upon compression up to 7%. The CBM shifts downward from K to a point around K and VBM shifts from the K-point to Γ-point. (**a**) Uniaxial tensile strain along zig-zag direction, (**b**) uniaxial tensile strain along arm-chair direction, (**c**) uniaxial compressive strain along zig-zag direction and (**d**) uniaxial compressive strain along arm-chair direction.

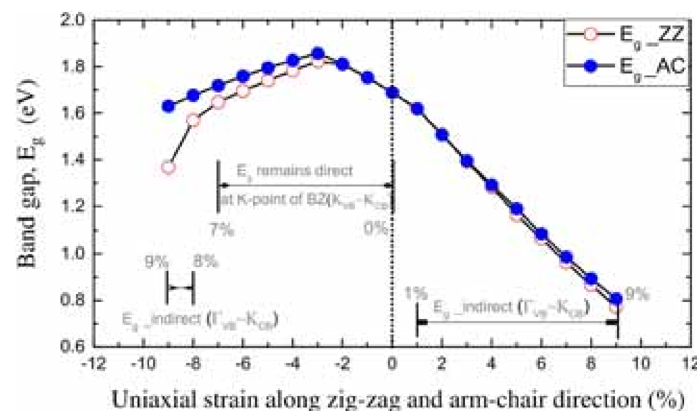

Figure 3. Variation in the band gap with uniaxial strain applied along zig-zag as well as arm-chair directions.

Table 1. Lattice scaling and variation in electronic band gap with strain along zig-zag (ZZ) and arm-chair (AC) directions; D = direct band gap, ID = indirect band gap.

	Uniaxial tensile strain @ ZZ direction		Uniaxial tensile strain @ AC direction		Uniaxial compressive strain @ ZZ direction		Uniaxial compressive strain @ AC direction	
Strain	Lattice parameter (Å)	Band gap (eV)	Lattice parameter (Å)	Band gap (eV)	Lattice parameter (Å)	Band gap (eV)	Lattice parameter (Å)	Band gap (eV)
0%	$a = 3.17$ $b = 5.50$	1.689 (D)	$a = 3.17$ $b = 5.50$	1.689 (D)	$a = 3.17$ $b = 5.50$	1.689 (D)	$a = 3.17$ $b = 5.50$	1.689 (D)
1%	$a = 3.21$ $b = 5.50$	1.620 (ID)	$a = 3.17$ $b = 5.55$	1.619 (ID)	$a = 3.14$ $b = 5.50$	1.753 (D)	$a = 3.17$ $b = 5.45$	1.753 (D)
2%	$a = 3.21$ $b = 5.50$	1.620 (ID)	$a = 3.17$ $b = 5.55$	1.619 (ID)	$a = 3.14$ $b = 5.50$	1.753 (D)	$a = 3.17$ $b = 5.45$	1.753 (D)
3%	$a = 3.24$ $b = 5.50$	1.508 (ID)	$a = 3.17$ $b = 5.61$	1.507 (ID)	$a = 3.11$ $b = 5.50$	1.81 (D)	$a = 3.17$ $b = 5.39$	1.812 (D)
4%	$a = 3.27$ $b = 5.50$	1.391 (ID)	$a = 3.17$ $b = 5.67$	1.396 (ID)	$a = 3.08$ $b = 5.50$	1.822 (D)	$a = 3.17$ $b = 5.34$	1.857 (D)
5%	$a = 3.30$ $b = 5.50$	1.282 (ID)	$a = 3.17$ $b = 5.72$	1.292 (ID)	$a = 3.05$ $b = 5.50$	1.783 (D)	$a = 3.17$ $b = 5.28$	1.827 (D)
6%	$a = 3.37$ $b = 5.50$	1.065 (ID)	$a = 3.17$ $b = 5.83$	1.086 (ID)	$a = 2.99$ $b = 5.50$	1.696 (D)	$a = 3.17$ $b = 5.17$	1.759 (D)
7%	$a = 3.40$ $b = 5.50$	0.956 (ID)	$a = 3.17$ $b = 5.89$	0.986 (ID)	$a = 2.95$ $b = 5.50$	1.648 (D)	$a = 3.17$ $b = 5.12$	1.719 (D)
8%	$a = 3.43$ $b = 5.50$	0.865 (ID)	$a = 3.17$ $b = 5.94$	0.893 (ID)	$a = 2.92$ $b = 5.50$	1.569 (ID)	$a = 3.17$ $b = 5.06$	1.676 (ID)
9%	$a = 3.46$ $b = 5.50$	0.772 (ID)	$a = 3.17$ $b = 5.99$	0.806 (ID)	$a = 2.89$ $b = 5.50$	1.367 (ID)	$a = 3.17$ $b = 5.01$	1.63 (ID)

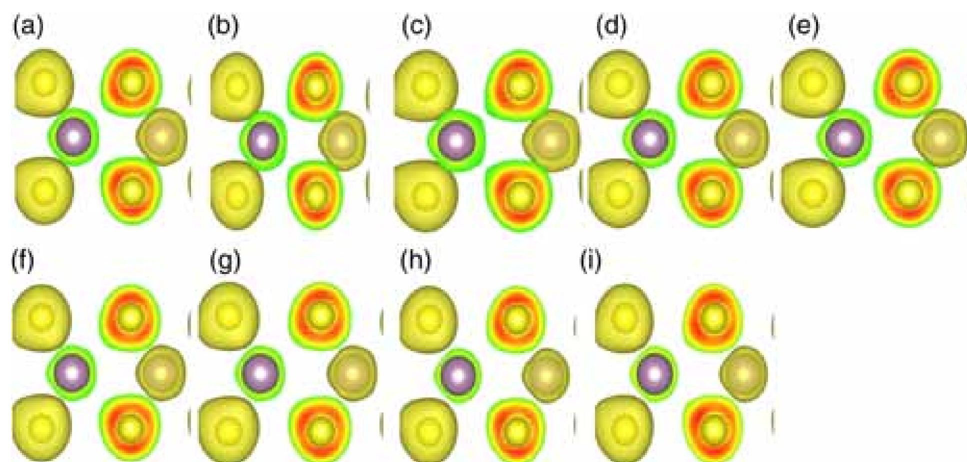

Figure 4. Electronic charge density at different levels of strain. **(a)** Strain-free condition, **(b)** for 5% and **(c)** for 9% uniaxial tensile strain applied along the zig-zag direction respectively, **(d)** for 5% and **(e)** for 9% for uniaxial tensile strain along the arm-chair direction respectively, **(f)** for 5% and **(g)** for 9% for uniaxial compressive strain along zig-zag direction respectively and **(h)** for 5% and **(i)** for 9% uniaxial compressive strain along the armchair direction respectively.

Table 2. Bader charge analysis of strain-free and uniaxially strained ML–MoS_2 nanosheet.

		Uniaxial tensile strain				Uniaxial compressive strain			
		Zig-zag direction		Arm-chair direction		Zig-zag direction		Arm-chair direction	
Strain	No strain 0%	5%	9%	5%	9%	5%	9%	5%	9%
Charge on Mo	4.3482e	4.3932e	4.3996e	4.3498e	4.3435e	4.3704e	4.3725e	4.3533e	4.3251e
(ΔQ)		(0.045e)	(0.0508e)	(0.0016e)	(−0.0047e)	(0.0222e)	(0.0243e)	(0.0051e)	(−0.0231e)
Charge on S	6.8195e	6.8034e	6.8031e	6.8182e	6.8157e	6.7999e	6.7941e	6.8169e	6.8334e
(ΔQ)		(−0.0161e)	(−0.0164e)	(−0.0013e)	(−0.0038e)	(−0.0196e)	(−0.0254e)	(−0.0026e)	(0.0139e)

ΔQ is the change in electronic charge with respect to the unstrained system.

as well as strained ML–MoS_2 nanosheets, as tabulated in table 2. From table 2, it is clear that the application of both types of uniaxial strain, is unable to bring about any considerable change in the atomic charges on Mo and S atoms. This is due to the fact that atomic motion is unhindered/unconstrained along the other direction where strain is not applied.

4. Conclusion

In summary, the variations in electronic properties of MoS_2–ML nanosheet with the application of uniaxial strain along two non-equivalent crystal directions have been studied. Tensile strain applied along the zig-zag direction induces the maximum effect: it tunes the band gap from 1.689 to 0.772 eV. In the case of compressive strain applied along the zig-zag direction, the band gap first increases to 1.822 eV at 3% of the applied strain and then decreases to 1.36 eV when the strain reaches 9%. Corresponding to uniaxial tensile strain applied along the zig-zag direction, the CBM shifts down vertically and remains around the K-point under strain, while the VBM shifts from K-point (direct) to Γ-point, makes the system indirect band-gap semiconductor and for uniaxial compressive strain applied along the zig-zag direction brings down the band gap to 1.648 eV, while keeping the band gap direct up to 7% of the strain. Similar observation has been made in the case of uniaxial strain along the arm-chair direction but the extent is less stiffer compared to the zig-zag one on modulating the electronic band gap which is an important observation derived from this finding.

Acknowledgements

Fellowship and infrastructural support from Department of Science & Technology, Government of India

and Institute of Nano Science and Technology respectively are gratefully acknowledged. The authors remain highly thankful to the Centre for Development in Advanced Computing-Pune for providing its supercomputing facilities on PARAM-YUVA-II.

References

[1] Q H Wang, K Kalantar-Zadeh, A Kis, J N Coleman and M S Strano, *Nat. Nanotechnol.* **7**, 699 (2012)
[2] A H Castro Neto, N M R Peres, K S Novoselov, A K Geim, F Guinea and A Neto, *Rev. Mod. Phys.* **81**, 109 (2009)
[3] K S Novoselov, D Jiang, F Schedin, T J Booth, V V Khotkevich, S V Morozov and A K Geim, *Proc. Natl Acad. Sci. USA* **102**, 10451 (2005)
[4] N V Podberezskaya, S A Magarill, N V Pervukhina and S V Borisov, *J. Struct. Chem.* **42**, 654 (2001)
[5] S Ahmad and S Mukherjee, *Graphene* **52**, 3 (2014)
[6] A M Jones, H Yu, N J Ghimire, S Wu, G Aivazian, J S Ross, B Zhao, J Yan, D G Mandrus, D Xiao, W Yao and X Xu, *Nat. Nanotechnol.* **8**, 634 (2013)
[7] A Splendiani, L Sun, Y Zhang, T Li, J Kim, C Y Chim, G Galli and F Wang, *Nano Lett.* **10**, 1271 (2010)
[8] A Kuc, N Zibouche and T Heine, *Phys. Rev. B* **83**, 245213 (2011)
[9] H Wang, L Yu, Y H Lee, W Fang, A Hsu, P Herring, M Chin, M Dubey, L J Li and J Kong, *Nano Lett.* **12**, 9 (2012)
[10] E Scalise, M Houssa, G Pourtois, V V Afanasev and A Stesmans, *Phys. E Low-Dimensional Syst. Nanostruct.* **56**, 416 (2014)
[11] W Wu, L Wang, Y Li, F Zhang, L Lin, S Niu, D Chenet, X Zhang, Y Hao, T F Heinz, J Hone and Z L Wang, *Nature* **514**, 470 (2014)
[12] Y T Wang *et al*, *Sci. Rep.* **5**, 8289 (2015)
[13] L J Hui, *Large area 2D transition metal dichalcogenides: Synthesis, chracterization and application of* MoS_2, Thesis (2014)
[14] Q Yue, J Kang, Z Shao, X Zhang, S Chang, G Wang, S Qin and J Li, *Phys. Lett. A* **376**, 1166 (2012)
[15] M Chhowalla, H S Shin, G Eda, L-J Li, K P Loh and H Zhang, *Nat. Chem.* **5**, 263 (2013)
[16] G Eda, T Fujita, H Yamaguchi, D Voiry, M Chen and M Chhowalla, *ACS Nano* **6**, 7311 (2012)
[17] F Guinea, M I Katsnelson and A K Geim, *Nat. Phys.* **6**, 30 (2010)
[18] T Kaewmaraya, A De Sarkar, B Sa, Z Sun and R Ahuja, *Comput. Mater. Sci.* **91**, 38 (2014)
[19] P Liu, A De Sarkar and R Ahuja, *Comput. Mater. Sci.* **86**, 206 (2014)
[20] Y Li, A De Sarkar, B Pathak and R Ahuja, *Appl. Phys. Lett.* **102**, 243905 (2013)
[21] T Hussain, T Adit Maark, A De Sarkar and R Ahuja, *Appl. Phys. Lett.* **101**, 1 (2012)
[22] W Kohn and L J Sham, *Phys. Rev.* **140**, A1133 (1965)
[23] P Hohenberg and W Kohn, *Phys. Rev.* **136**, B864 (1964)
[24] C Steffen, K Thomas, U Huniar, A Hellweg, O Rubner and A Schroer, *J. Comput. Chem.* **31**, 2967 (2010)
[25] G Kresse and J Hafner, *Phys. Rev. B* **49**, 14251 (1994)
[26] G Kresse and D Joubert, *Phys. Rev. B* **59**, 1758 (1999)
[27] P E Blchl, *Phys. Rev. B* **50**, 953 (1994)
[28] J P Perdew and Y Wang, *Phys. Rev. B* **45**, 13244 (1992)
[29] J Perdew, K Burke and Y Wang, *Phys. Rev. B* **54**, 16533 (1996)
[30] H-P Komsa and A V Krasheninnikov, *Phys. Rev. B* **88**, 085318 (2013)
[31] P Johari and V B Shenoy, *ACS Nano* **6**, 5449 (2012)
[32] K Mak, C Lee, J Hone, J Shan and T Heinz, *Phys. Rev. Lett.* **105**, 136805 (2010)